THE JOURNAL OF PHYSICAL CHEMISTRY LETTERS
A JOURNAL OF THE AMERICAN CHEMICAL SOCIETY

pubs.acs.org/JPCL

Letter

Role of Dielectric Screening in Calculating Excited States of Solvated Azobenzene: A Benchmark Study Comparing Quantum Embedding and Polarizable Continuum Model for Representing the Solvent

Chandrima Chakravarty,[§] Huseyin Aksu,[§] Jessica A. Martinez B., Pablo Ramos, Michele Pavanello, and Barry D. Dunietz*

Cite This: *J. Phys. Chem. Lett.* 2022, 13, 4849−4855

Read Online

ACCESS | Metrics & More | Article Recommendations | Supporting Information

ABSTRACT: The low energy excited states of the conformational isomers of solvated azobenzene are calculated with several DFT methods accounting for the solute−solvent interaction implicitly with the polarizable continuum model or explicitly with subsystem DFT. For the latter, embedding potentials are calculated for 21 sampled snapshots of the solvent molecules. First, we find that accounting for the solvent implicitly or explicitly has little effect on the predicted cis−trans S_1 excitation energy gap. Second, we find that azobenzene's S_1 cis and trans energies are accurate as long as a screened range-separated hybrid exchange-correlation functional is employed. Finally, we also tested a simplified workflow whereby a single, averaged, embedding potential is used. Unfortunately, we find larger deviations against the experiment for the simplified workflow. This highlights a basic flaw in the approach, where the time scale of solvent averaging is much longer than that of the solute's electronic polarization.

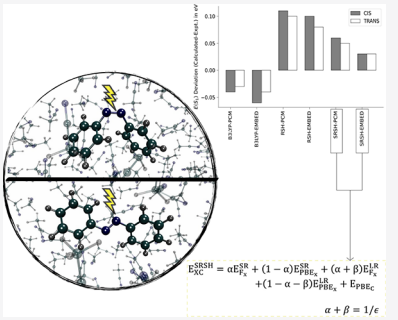

Chemical and photochemical reactions occur primarily in molecular condensed phases. That is, liquid solutions where a photoactive solute is the molecule of interest, surrounded by a bulk of liquid solvent. Naturally, a long-standing problem in quantum chemistry has been to find a computationally cheap yet accurate method for accounting for solute−solvent interactions. Both implicit and explicit solvent methods exist. In particular, implicit solvent models, such as polarizable continuum model (PCM) and conductor like screening model (COSMO),[1] are workhorses of computational chemists. Among the explicit solvent models, quantum mechanical (QM) based embedding has emerged in recent years as a powerful alternative.[2−6] QM embedding provides for a rigorous framework to simplify complex systems, whereby a molecular core is typically defined (e.g., the solute), surrounded by a much larger molecular environment (e.g., the solvent). Often the core is treated at a higher level of electronic structure theory than the surroundings.[7] The simplest workflow for an explicit treatment of the solvent is the so-called QM/MM method in which a QM calculation of the core region takes place in the field of point-like multipoles residing in the environment, i.e., the molecular mechanics region.[8−14] However, the quality of the environment representation in QM/MM calculations is limited not only by the suitability of the force field but also by nonelectrostatic interactions (such as Pauli repulsion). Their neglect can induce numerical instabilities.[6]

Quantum embedding approaches address these issues by extending QM calculations to large systems, representing also the environment quantum mechanically.[15,16] Wesolowski and Warshel showed that the environment can formally be represented through the inclusion of an additional potential in the Kohn−Sham equations of an embedded subsystem[16] and in particular can be used for addressing solvent molecules affecting a solute's electronic structure and dynamics.

Recently, calculations based on the screened range separated hybrid (SRSH) functionals in PCM were shown to provide excellent ground state transport properties.[17] In SRSH-PCM the energies of the frontier orbitals correspond well to ionization potential (IP) and electron affinity (EA) of molecular systems in the condensed phase. SRSH-PCM was also benchmarked for reproducing measured excited states energies and in particular for charge transfer states in solvated donor−acceptor systems.[18] Followup studies based on SRSH-PCM provided unique insight on spectral trends in photosystems and organic semiconducting model systems.[19−25]

In this study we employ the SRSH exchange-correlation (xc) functional for computing the electronic structure of azobenzene (AB) dissolved in an acetonitrile solution. SRSH-PCM as well as SRSH-EMBED (i.e., AB treated by SRSH embedded by

Received: April 4, 2022
Accepted: May 18, 2022
Published: May 26, 2022

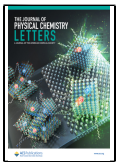

https://doi.org/10.1021/acs.jpclett.2c00982
J. Phys. Chem. Lett. 2022, 13, 4849−4855

subsystem DFT acetonitrile environment) averaged over a representative set of solvent configurations are compared to experimental excitation energies. We also provide comparisons to excitation energies obtained using other xc functionals such as a traditional hybrid functional, B3LYP, and the corresponding unscreened RSH functional. By comparing the DFT-EMBED excitation energies to corresponding PCM values we provide an important benchmark to understand the means required for representing reliably at moleular resolution the solvent effects. In addition, the dynamical response of the solvent is addressed by two nonequilibrium PCM formalisms (ptLR and ptSS, *vide infra*).[26−29]

We investigate the lowest excited state S_1 for both the cis and trans isomers of AB. The photoisomerization reaction in AB has drawn wide research attention as a proof-of-concept system[30−32] for the design of molecular photoswitches opening the door to a wide range of applications in the fields of drug delievery,[33,34] DNA/RNA engineering,[32,35] and photoisomerization.[36] The conformational isomerization in AB derivatives occurs for light in the UV to visible wavelength. To achieve an optimal selective yield of a particular isomer, the photoexciting radiation must be tuned to the corresponding conformer excitation energy, requiring a sufficiently large cis−trans energy gap. Therefore, to aid relevant material design efforts, the cis−trans energy gap of the solvated AB system has to be resolved in high accuracy.

Recently, the Bethe Salpeter equation (BSE) coupled with embedding calculations using a similar RSH functional as employed below were shown to perform relatively well in describing the gap energies but appear to overestimate the S_1 energies in comparison to experimental values.[37] We show that the much simpler SRSH formulation appears to achieve a good effective treatment of the environment polarization effect on the electron−electron interactions at long ranges due to the solvent. As we will show below, the calculated S_1 SRSH energies are in agreement with the experimental values within 0.03 eV.

In this work, the success of the SRSH-PCM and SRSH-EMBED methods is shown for AB, a prototypical system of photochemistry. As the average embedding-based excited state energies are found to be within 0.03 eV of the corresponding PCM energies, we demonstrate that the relatively small-sized sample of 21 solvent configurations chosen from the subsystem DFT *ab initio* molecular dynamics (AIMD) represents well the solvent at a molecular resolution. The quantum embedding framework presented here constitutes an important stepping stone for developing physically meaningful computational models of electronic excited potential energy surfaces in molecular condensed phases. Here, the calculated electronic states address at molecular resolution the role of the environment in condensed-phase molecular systems. Such a resolution is required, for example, to investigate biological chemical reactions such as an enzymatic reactive core within its protein matrix.

We investigate computationally the lowest excited state S_1 energy, $E(S_1)$, of both isomers of AB solvated in acetonitrile, for which there are experimental values to compare against. The molecular geometries of both cis and trans AB are optimized using a dispersion corrected functional, the ωB97X-D,[38] accounting for the effect of the solvent using PCM[1,39] with a scalar dielectric constant that corresponds to the acetonitrile solvent (ϵ = 37.5[40]). Optimized geometries of the cis and trans AB isomers are shown in Figure 1 with the coordinates listed in the Supporting Information (SI). We also point out that the two isomers are associated with effectively the same zero point vibrational correction energy.

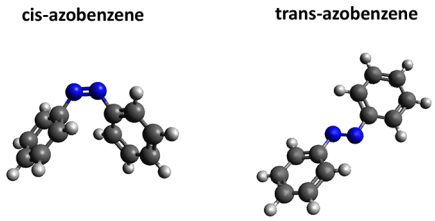

Figure 1. Azobenzene's cis and trans isomers considered in this work.

Excitation energies are obtained at the TDDFT level based on an optimally tuned RSH functional, the LRC-ωPBE,[41] its corresponding SRSH functional,[17] and the B3LYP functional. RSH or long-range-corrected functionals are found to address well the fundamental orbital gap caveat associated with traditional DFT calculations.[41−46] RSH-PCM has also been employed successfully in TDFFT calculations of condensed-phase excited state energies[46−48] through postprocessing energy correction terms. Additionally, in this work to further improve the treatment of the condensed phase, the exact exchange is screened at the long-range (LR) by resetting the functional parameters according to the same dielectric constant that characterizes the solvent in PCM. In this way, the solute's electron−electron interaction at long range is screened by a dielectric constant consistent with the PCM solvent polarization. Indeed, SRSH-PCM is found to reliably address the frontier orbital renormalization in the condensed phase through a self-consistent environment polarization,[17] and excitations calculated using TDDFT with SRSH-PCM have been benchmarked successfully.[18,22]

To implement the SRSH functional, a generalized partition of the Coulomb interaction operator, using the error function,[49] is invoked, where

$$\frac{1}{r} = \frac{\alpha + \beta\ \mathrm{erf}(\omega r)}{r} + \frac{1 - \alpha - \beta\ \mathrm{erf}(\omega r)}{r} \tag{1}$$

Here, r is the electron-interaction distance, ω is a system-dependent range switching parameter, and α and β are functional parameters. A general exchange correlation expression then results by using Fock exchange for the first term in eq 1 and the semilocal PBE exchange for the second term:

$$E_{XC}^{SRSH} = \alpha E_{F_X}^{SR} + (1 - \alpha)E_{PBE_X}^{SR} + (\alpha + \beta)E_{F_X}^{LR} + (1 - \alpha - \beta)E_{PBE_X}^{LR} + E_{PBE_C} \tag{2}$$

where the subscripts "X" and "C" denote exchange and correlation, the subscripts "F" and "PBE" denote Fock and PBE exchange, and the superscripts "SR" and "LR" denote short-range and long-range. In SRSH, β is reset according to $\alpha + \beta = 1/\epsilon$, with a preset value for α, which determines the fraction of Fock exchange in the SR. For a given α, the range-separation parameter is obtained by optimal tuning (OT) at the gas phase (ϵ = 1), minimizing the error measure, $J(\omega)$, with respect to the range-switching parameter, ω, where

$$J(\omega) = [\varepsilon_{\mathrm{HOMO}}(\omega) + \mathrm{IP}(\omega)]^2 + [\varepsilon_{\mathrm{LUMO}}(\omega) + \mathrm{EA}(\omega)]^2 \tag{3}$$

Here, $\varepsilon_{\mathrm{HOMO}}$ and $\varepsilon_{\mathrm{LUMO}}$ are the energies of the highest occupied molecular orbital (HOMO) and the lowest

https://doi.org/10.1021/acs.jpclett.2c00982
J. Phys. Chem. Lett. 2022, 13, 4849−4855

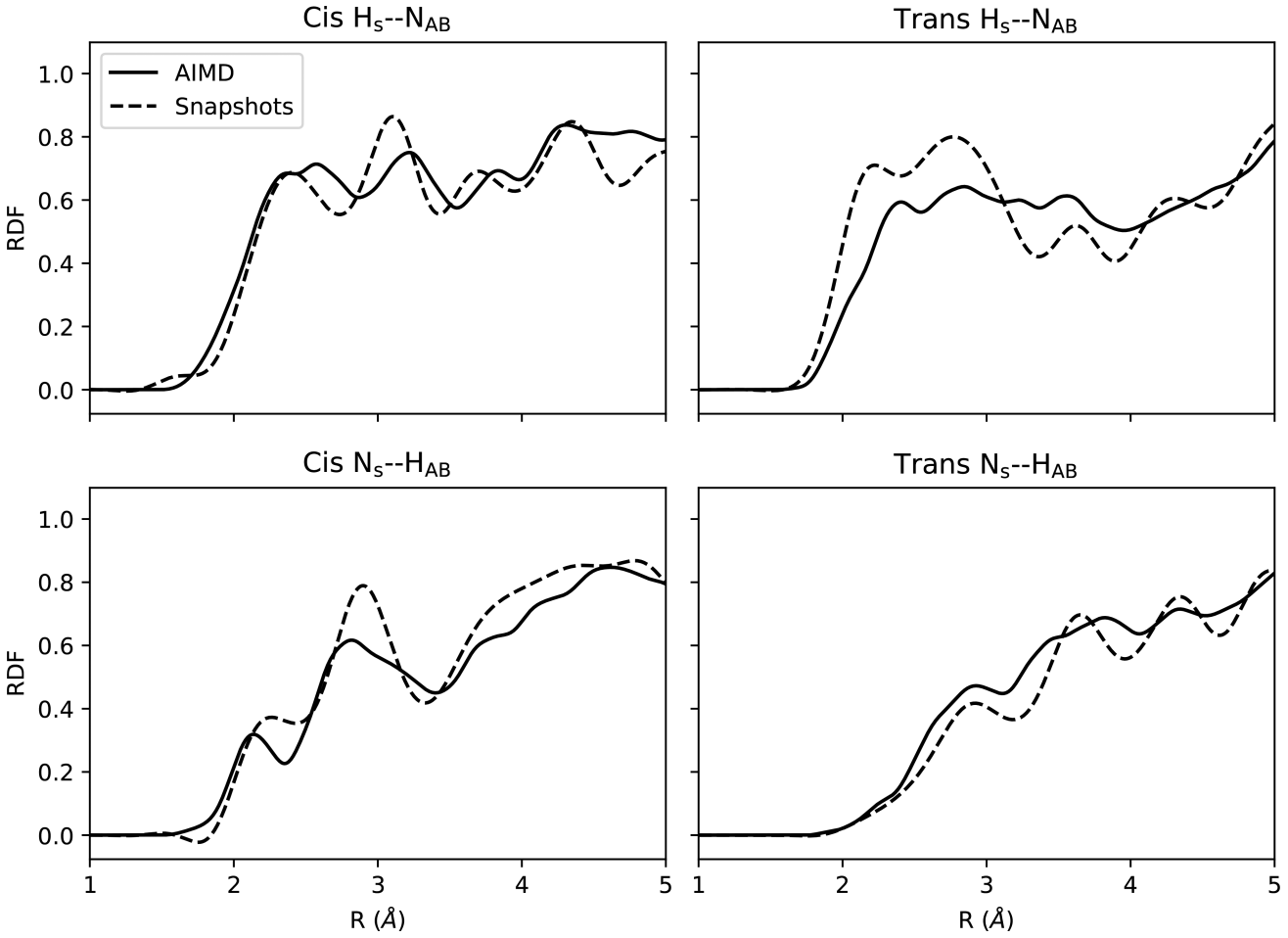

Figure 2. RDFs of H−N intermolecular distances, where the atoms either belong to AB (subscript AB) or to the acetonitrile solvent molecules (subscript s).

unoccupied molecular orbital (LUMO), respectively. IP and EA represent the vertical ionization energies of the system. Further condensed phase tuning can be done by repeating the process upon tuning α to minimize a similar error measure within PCM

$$J(\alpha) = [\varepsilon^{PCM}_{\mathrm{HOMO}}(\alpha) + IP^{\mathrm{PCM}}(\alpha)]^2 + [\varepsilon^{PCM}_{\mathrm{LUMO}}(\alpha) + EA^{\mathrm{PCM}}(\alpha)]^2 \tag{4}$$

Particularly, as α is tuned, the β parameter is reset such that their sum remains equal to the inverse of the dielectric constant.

For the SRSH-PCM results, the PCM-based optimal values of α are 0.326 and 0.346 for the trans and cis isomers, respectively. The range separation parameter, ω, is 142 for both isomers with their corresponding PCM tuned α value. For completion we also report results based on α = 0.2, referred to as SRSH-PCM(0.2), and which corresponds to switching values, ω, of 177 and 189 for cis and trans, respectively.

To provide an atomistic description of solute−solvent interactions, we run simulations with 85 explicit acetonitrile solvent molecules by AIMD based on density embedding implemented in the embedded Quantum ESPRESSO (eQE) package.[50,51] In density embedding, the total electron density, $\rho(\mathbf{r})$, is given as a sum of subsystem contributions,

$$\rho(\mathbf{r}) = \sum_{I=1}^{N_S} \rho_I(\mathbf{r}) \tag{5}$$

with N_S being the total number of subsystems.

Each of the subsystem electron densities is determined variationally by solving the following self-consistent Kohn−Sham (KS)-like equation, one per subsystem. Namely,

$$\left[\frac{-\nabla^2}{2} + v^I_{KS}(\mathbf{r}) + v^I_{\mathrm{emb}}(\mathbf{r})\right]\phi_{(i)I}(\mathbf{r}) = \varepsilon_{(i)I}\phi_{(i)I}(\mathbf{r}) \tag{6}$$

where the effective KS Hamiltonian of each subsystem, I, contains the KS potential as if the subsystem was isolated, $v^I_{KS}(\mathbf{r})$, and the embedding potential, $v^I_{\mathrm{emb}}(\mathbf{r})$, which encodes the interactions with all other subsystems. The embedding potential for subsystem I takes the form

$$v^I_{\mathrm{emb}}(\mathbf{r}) = \sum_{J\neq I}^{N_S}\left[\int \frac{\rho_J(\mathbf{r}')}{|\mathbf{r}-\mathbf{r}'|}\,\mathrm{d}\mathbf{r}' - \sum_{\alpha\in J}\frac{Z_\alpha}{|\mathbf{r}-\mathbf{R}_\alpha|}\right] + \underbrace{\frac{\delta T_s[\rho]}{\delta\rho(\mathbf{r})} - \frac{\delta T_s[\rho_I]}{\delta\rho_I(\mathbf{r})}}_{v^{\mathrm{nad}}_{T_s}(\mathbf{r})} + \underbrace{\frac{\delta E_{\mathrm{xc}}[\rho]}{\delta\rho(\mathbf{r})} - \frac{\delta E_{\mathrm{xc}}[\rho_I]}{\delta\rho_I(\mathbf{r})}}_{v^{\mathrm{nad}}_{\mathrm{xc}}(\mathbf{r})} \tag{7}$$

where $v^{\mathrm{nad}}_{T_s}$ and $v^{\mathrm{nad}}_{\mathrm{xc}}$ are the nonadditive kinetic energy and nonadditive exchange-correlation terms, respectively. The

https://doi.org/10.1021/acs.jpclett.2c00982
J. Phys. Chem. Lett. 2022, 13, 4849−4855

subsystem DFT simulations are carried out with eQE,[50,51] which computes the nonadditive terms on a Cartesian grid in real space exploiting fast Fourier transform for the computation of electron density gradients needed for the evaluation of the nonadditive functionals. Details about the implementation and benchmark timings are available elsewhere.[50,51]

We run independent dynamics for the cis and trans isomers of AB, each solvated by 85 acetonitrile molecules with a frozen solute conformation. In density embedding,[4−6] every nonbonded fragment is treated as a quantum subsystem. Thus, in the AIMD we have a total of 86 subsystems. All calculations were run at the Γ point. We used ultrasoft pseudopotentials (pbe-rrkjus-gipaw-dc.UPF from the main Quantum ESPRESSO library), and 40 and 400 Ry are the energy cutoffs for the plane wave expansion of the molecular orbitals and the charged density, respectively. For the simulation, we use 4 processors per subsystem, totaling 344 processors.

Due to the need to consider molecular condensed phases, the AIMD simulations are carried out in a cubic simulation cell with a lattice constant of a = 19.54 Å. The temperature was set to 340 K ± 30 K using velocity rescaling, and the dynamics was driven by the Verlet algorithm with a time step of 15 au (1 au = $2.4118884 \times 10^{-17}$ s). We run 7218 and 7026 steps for cis and trans AB, respectively. The first 3502 (5114) steps for cis (trans) are needed for equilibration and, therefore, were discarded from the subsequent analyses. The potential energy of the simulation trajectories is plotted in SI Figure S1.

Twenty-one (21) snapshots are selected from each of the cis and trans trajectories and verified for probing the solvent conformations as described below. We compute the embedding potential[50] for the AB molecules in each snapshot using eq 7 by first representing it on eQE's Cartesian grid and, in a second step, splining it onto the atom-centered Lebedev DFT grid for the Q-Chem calculation of the excited states employing a Gaussian atomic orbitals basis set. The 6-31G* basis set was employed. The nonadditive potentials are calculated using the PBE functional[52] for the exchange-correlation and revAPBEK functional[53] for the kinetic energy.

To verify that the snapshot sample represents well the solvent space, we consider the radial distribution functions (RDFs) of intermolecular distances between acetonitrile's hydrogens (H_s) and AB's nitrogens (N_{AB}) as well as AB's H (H_{AB}) and acetonitrile's N (N_s) as reported in Figure 2 for the cis and trans isomers. We compare the RDFs from the entire AIMD trajectories to the ones limited to the selected snapshots to confirm that the snapshots, while quite limited in number, sample well the ensemble of solvent configurations. Specifically, the onsets of the RDFs are similar (roughly 1.6 Å), and the main peaks in the first coordination shells are also semiquantitatively reproduced by the selected snapshots.

With the embedding potentials at hand, we compare the excitation energy calculated with PCM to the average of TDDFT calculations in the presence of the embedding potentials, one for each of the 21 snapshots (EMBED, hereafter). Additionally, inspired by works of Wesolowski and co-workers,[54,55] we also compute the excitation energies obtained using an averaged embedding potential (AVE-EMBED, hereafter). The AVE-EMBED values embody the following approximation for the excitation energy,

$$\langle \Delta E[v_{\mathrm{emb}}] \rangle \approx \Delta E[\langle v_{\mathrm{emb}} \rangle] \tag{8}$$

The advantage of using the averaged embedding potential is that only a single TDDFT calculation is required. We note that earlier implementations to obtain the above average employed an averaged solvent density from which an embedding potential was derived.[54,55]

A question may arise concerning the dynamical response to an electronic state excitation of the solvent that can be significant.[2,56,57] To address this point, we employ nonequilibrium PCM that incorporates the solvent's response by the dielectric polarization derived from the solvent's optical dielectric constant.[26−29] More specifically, we carry out a perturbation theory state-specific (ptSS) version of nonequilibrium PCM following the implementation by Herbert and co-workers.[39,58,59] There is an intermediate level of solvent response for nonequilibrium PCM in Q-Chem,[60] namely, perturbation theory linear response (ptLR),[39] derived from ref 61. Both ptLR and ptSS energies are reported below for the different DFT levels as LR-PCM and SS-PCM, respectively, and compared to the excitation energies computed with the PCM reaction field corresponding to the ground state. We point out that the nonequilibrium ptSS and ptLR corrected energies include only the electronic (fast) contributions to the polarization in calculating the solvent reaction field. In the equilibrium limit the solvent reaction field is assumed to be fully relaxed following both the electronic (fast) and the nuclear (slow) contributions under the polarization of the relevant state.

The calculated excitation energies, $E(S_1)$, are listed in Table 1. The deviations of calculated energies from the measured values, $\Delta E_{S1}^{\mathrm{exp}}$, that are listed in the table are also graphically represented in Figure 3 for ease of comparison. We start by considering the excitation energies obtained by embedded

Table 1. Solvated cis and trans AB Electronic Excitation Energies of the First State, $E(S_1)$, Calculated at the Various Levels with PCM and Density Embedding[a]

	cis		trans		
methods	$E(S_1)$	$\Delta E_{S1}^{\mathrm{exp}}$	$E(S_1)$	$\Delta E_{S1}^{\mathrm{exp}}$	ΔE^{g}
B3LYP-PCM	2.84	−0.04	2.76	−0.03	0.08
B3LYP-LR-PCM	2.82	−0.06	2.75	−0.04	0.07
B3LYP-SS-PCM	2.84	−0.04	2.75	−0.04	0.09
B3LYP-EMBED	2.82	−0.06	2.75	−0.04	0.07
AVE-EMBED	2.84		2.67		
RSH-PCM	2.99	0.11	2.89	0.10	0.10
RSH-LR-PCM	2.98	0.10	2.88	0.09	0.10
RSH-SS-PCM	2.99	0.11	2.88	0.09	0.11
RSH-EMBED	2.98	0.10	2.87	0.08	0.11
AVE-EMBED	3.00		2.80		
SRSH-PCM	2.94	0.06	2.84	0.05	0.10
SRSH-LR-PCM	2.92	0.04	2.82	0.03	0.10
SRSH-SS-PCM	2.93	0.05	2.83	0.04	0.10
SRSH-EMBED	2.91	0.03	2.82	0.03	0.09
AVE-EMBED	2.94		2.75		
BSE[37]	2.95	0.07	2.83	0.04	0.12
experiment[63]	2.88	–	2.79	–	0.09

[a]The embedding excitation energies are averaged over the 21 snapshots of solvent configurations. Also listed are the benchmark experimental values and BSE calculated energies. ΔE^{g} is the cis−trans energy gap, and $\Delta E_{S1}^{\mathrm{exp}}$ is the deviation of the calculated $E(S_1)$ from the experimental value (eV). For each level we also list as the AVE-EMBED the S_1 energies computed with the approximation in eq 8.

https://doi.org/10.1021/acs.jpclett.2c00982
J. Phys. Chem. Lett. 2022, 13, 4849−4855

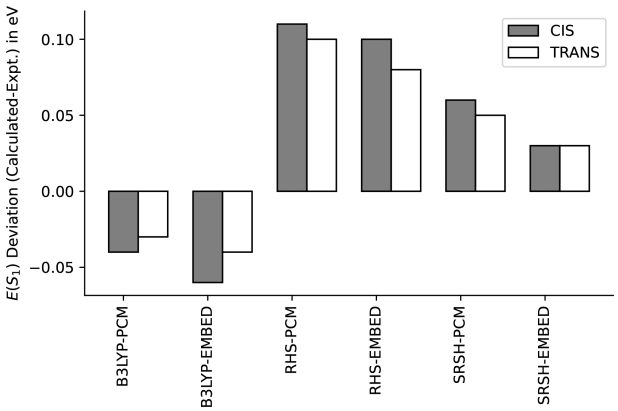

Figure 3. Deviation of the calculated $E(S_1)$ from the measured energies at the different DFT levels. (DFT-EMBED is the average of the embedded field affected energies.)

TDDFT calculations averaged over the 21 snapshots for each isomer. The detailed list of the snapshot excitation energies is provided in SI Table S1. These underestimate the experiment at the B3LYP level by about 0.05 eV and overestimate the experiment at the RSH level by around 0.1 eV. Employing SRSH, the excitation energies for both cis and trans deviate from the experiment by 0.03 eV. We attribute these trends to the success of the SRSH in addressing the polarizing environment consistently as demonstrated well in several benchmark studies.[17,18,22,62] The cis−trans SRSH energy gap, ΔE^g, based on the averaged embedded energies is 0.09 eV and is in excellent agreement with the measured 0.09 eV gap. SRSH(0.2) $E(S_1)$ energies (listed in SI Table S2) are found to be significantly lower at 2.79 and 2.68 eV, for cis and trans, respectively, overestimating the measured gap by 0.02 eV. This highlights the importance for carefully considering the functional parameter space in SRSH calculations.

The averaged embedding energy, DFT-EMBED, is in agreement of 0.03 eV with the corresponding PCM value, DFT-PCM, for all the considered DFT levels. In all the cases we find that the LR-PCM value is within 0.01 eV of the EMBED value. The LR-PCM excitation energies are lower by 0.01−0.02 eV than the zeroth order PCM values. We point out the SS-PCM values, addressing the nonequilibrium effects due to fast, electronic contributions of the solvent dielectric susceptibility, that appear to increase the excitation energy over that of the LR-PCM energy more so for the cis isomer (by up to 0.02 eV) than the trans isomer (by up to 0.01 eV). However, we find that accounting for nonequilibrium solvation at the SS-PCM level results in an overall negligible contribution to the computed excitation energies. Noted is the cis−trans LR-PCM energy gap that is in excellent agreement with the measured gap for SRSH and RSH at 0.10 eV, whereas for B3LYP it is at 0.07 eV. We also point out that the BSE/GW calculations overestimate $E(S_1)$ by 0.07 and 0.04 eV for cis and trans over the experimental values, which result with an overestimated cis−trans gap of 0.12 eV.[37]

As a last point we compare the calculated excitation energies using the alternative method based on averaged embedding potentials in Table 1 listed as AVE-EMBED following eq 8. For the three considered xc functionals we find that AVE-EMBED is 0.02−0.03 eV above the TDDFT averaged value for the cis isomer. However, a larger discrepancy is noted for the trans isomer, where the AVE-EMBED is 0.07−0.08 eV lower than the TDDFT-averaged energy. This is consistent with the notion that the AVE-EMBED values are an approximation.

We computed the low-lying excitation energies of the cis and trans isomers of AB in acetonitrile solvent. To represent the solvent, we employed two methods: Continuum embedding by using the PCM model and density embedding by using subsystem DFT.

Having computed the embedding potentials for 21 snapshots of the solvent molecules, the average excitation energies from the 21 embedded TDDFT calculations are compared to mean field PCM energies and to the experiment. The calculated cis−trans energy gap by embedded TDDFT and PCM are found to be in excellent agreement with the experiment provided that range-separated hybrid functionals are employed. Specifically, the experimental cis−trans energy gap is 0.09 eV, which compares favorably with 0.10 eV using the SRSH and RSH frameworks and less so with B3LYP (0.07 eV).

The SRSH excitation energies are the closest to experimental values deviating only by 0.03 eV, whereas the B3LYP energies underestimate the experiment by 0.06 eV for the cis and 0.04 eV for the trans isomer. The corresponding RSH energies, instead, overestimate the experiment by close to about 0.1 eV. These trends indicate that accounting for solvent screening in the solute's electron−electron interaction via the SRSH framework leads to a correct description of the low-lying excited state of azobenzene in solution. SRSH is found to be successful whether coupled with PCM or with density embedding for addressing the solute−solvent interactions. Interestingly, with all considered DFT levels we find good agreement within 0.03 eV between the EMBED and the corresponding PCM energies, highlighting the success of both PCM and the quantum embedding framework, as well as the sampling scheme chosen for this work.

■ ASSOCIATED CONTENT

Supporting Information

The Supporting Information is available free of charge at https://pubs.acs.org/doi/10.1021/acs.jpclett.2c00982.

Individual S_1 embedded energies at the various snapshots, atomic Cartesian coordinates of the optimized cis and trans AB, RSH and SRSH with α = 0.2 first excitation energy $E(S_1)$, individual S_1 embedded energies at the various snapshots, atomic Cartesian coordinates of the optimized cis and trans AB, and total energy and potential energy across the whole AIMD simulation for both cis and trans isomers (PDF)

■ AUTHOR INFORMATION

Corresponding Author

Barry D. Dunietz − *Department of Chemistry and Biochemistry, Kent State University, Kent, Ohio 44242, United States;* orcid.org/0000-0002-6982-8995; Email: bdunietz@kent.edu

Authors

Chandrima Chakravarty − *Department of Chemistry and Biochemistry, Kent State University, Kent, Ohio 44242, United States*

Huseyin Aksu − *Department of Chemistry and Biochemistry, Kent State University, Kent, Ohio 44242, United States; Computational Physics Laboratory, Department of Physics,*

https://doi.org/10.1021/acs.jpclett.2c00982
J. Phys. Chem. Lett. 2022, 13, 4849−4855

Pamukkale University, 20010 Denizli, Turkey; orcid.org/0000-0001-9463-3236

Jessica A. Martinez B. − *Department of Chemistry, Rutgers University, Newark, New Jersey 07102, United States*

Pablo Ramos − *Department of Chemistry, Rutgers University, Newark, New Jersey 07102, United States*

Michele Pavanello − *Department of Chemistry, Rutgers University, Newark, New Jersey 07102, United States;* orcid.org/0000-0001-8294-7481

Complete contact information is available at: https://pubs.acs.org/10.1021/acs.jpclett.2c00982

Author Contributions

§(C.C. and H.A.) These authors contributed equally to this work.

Notes

The authors declare no competing financial interest.

Embedding potentials are available on Zenodo at the following DOI: 10.5281/zenodo.6397679.

■ ACKNOWLEDGMENTS

B.D.D. is grateful for support from the U.S. Department of Energy, Office of Basic Energy Sciences, under Award Number DE-SC0016501. We are thankful to the Ohio supercomputer[64] and the Kent State University College of Arts and Sciences for computing facilities and making the resources available to complete the reported research. M.P., P.R., and J.A.M.B. are supported by the U.S. Department of Energy, Office of Basic Energy Sciences, under Award Number DE-SC0018343 and by the National Science Foundation Grants CHE-2154760 and OAC-1931473. We thank the Office of Advanced Research Computing at Rutgers for providing access to the Amarel cluster. We are also grateful to Zheng Pei and Yihan Shao for helping to set up the Q-Chem program package for density embedding calculations.

■ REFERENCES

(1) Tomasi, J.; Mennucci, B.; Cammi, R. Quantum Mechanical Continuum Solvation Models. *Chem. Rev.* **2005**, *105*, 2999−3094.

(2) Neugebauer, J. Chromophore-Specific Theoretical Spectroscopy: From Subsystem Density Functional Theory to Mode-Specific Vibrational Spectroscopy. *Phys. Rep.* **2010**, *489*, 1−87.

(3) Severo Pereira Gomes, A.; Jacob, C. R. Quantum-Chemical Embedding Methods for Treating Local Electronic Excitations in Complex Chemical Systems. *Annu. Rep. Prog. Chem., Sect. C: Phys. Chem.* **2012**, *108*, 222−277.

(4) Krishtal, A.; Sinha, D.; Genova, A.; Pavanello, M. Subsystem Density-Functional Theory as an Effective Tool for Modeling Ground and Excited States, their Dynamics, and Many-Body Interactions. *J. Phys.: Condens. Matter J. Phys.: Condens. Matter* **2015**, *27*, 183202.

(5) Jacob, C. R.; Neugebauer, J. Subsystem Density-Functional Theory. *WIREs Comput. Mol. Sci.* **2014**, *4*, 325−362.

(6) Wesolowski, T. A.; Shedge, S.; Zhou, X. Frozen-Density Embedding Strategy for Multilevel Simulations of Electronic Structure. *Chem. Rev.* **2015**, *115*, 5891−5928.

(7) Wasserman, A.; Pavanello, M. Quantum Embedding Electronic Structure Methods. *Int. J. Quantum Chem.* **2020**, *120*, e26495.

(8) Jurinovich, S.; Pescitelli, G.; Di Bari, L.; Mennucci, B. A TDDFT/MMPol/PCM Model for the Simulation of Exciton-Coupled Circular Dichroism Spectra. *Phys. Chem. Chem. Phys.* **2014**, *16*, 16407−16418.

(9) Loco, D.; Lagardère, L.; Caprasecca, S.; Lipparini, F.; Mennucci, B.; Piquemal, J.-P. Hybrid QM/MM Molecular Dynamics with AMOEBA Polarizable Embedding. *J. Chem. Theory Comput.* **2017**, *13*, 4025−4033.

(10) Warshel, A.; Levitt, M. Theoretical Studies of Enzymic Reactions: Dielectric, Electrostatic and Steric Stabilization of the Carbonium ion in the Reaction of Lysozyme. *J. Mol. Biol.* **1976**, *103*, 227−249.

(11) Lin, H.; Truhlar, D. G. QM/MM: What Have We Learned, Where Are We, And Where Do We Go From Here? *Theor. Chem. Acc.* **2007**, *117*, 185.

(12) Senn, H. M.; Thiel, W. QM/MM Methods for Biomolecular Systems. *Angew. Chem., Int. Ed.* **2009**, *48*, 1198−1229.

(13) Brunk, E.; Rothlisberger, U. Mixed Quantum Mechanical/Molecular Mechanical Molecular Dynamics Simulations of Biological Systems in Ground and Electronically Excited States. *Chem. Rev.* **2015**, *115*, 6217−6263.

(14) Morton, S. M.; Silverstein, D. W.; Jensen, L. Theoretical studies of plasmonics using electronic structure methods. *Chem. Rev.* **2011**, *111*, 3962−3994.

(15) Cortona, P. Self-Consistently Determined Properties of Solids Without Band-Structure Calculations. *Phys. Rev. B* **1991**, *44*, 8454−8458.

(16) Wesolowski, T. A.; Warshel, A. Frozen Density Functional Approach for Ab Initio Calculations of Solvated Molecules. *J. Phys. Chem.* **1993**, *97*, 8050.

(17) Bhandari, S.; Cheung, M.; Geva, E.; Kronik, L.; Dunietz, B. D. Fundamental Gaps of Condensed-Phase Organic Semiconductors From Single-Molecule Polarization-Consistent Optimally Tuned Screened Range-Separated Hybrid Functionals. *J. Chem. Theory Comput.* **2018**, *14*, 6287−6294.

(18) Bhandari, S.; Dunietz, B. D. Quantitative Accuracy in Calculating Charge Transfer State Energies in Solvated Molecular Dimers Using Screened Range Separated Hybrid Functional Within a Polarized Continuum Model. *J. Chem. Theory Comput.* **2019**, *15*, 4305.

(19) Song, Y.; Schubert, A.; Maret, E.; Burdick, R. K.; Dunietz, B. D.; Geva, E.; Ogilvie, J. P. Vibronic Structure of Photosynthetic Pigments Probed by Polarized Two-dimensional Electronic Spectroscopy and ab initio Calculations. *Chem. Sci.* **2019**, *10*, 8143−8153.

(20) Aksu, H.; Schubert, A.; Geva, E.; Dunietz, B. D. Explaining Spectral Asymmetries and Excitonic Characters of the Core Pigment Pairs in the Bacterial Reaction Center Using Screened Range-Separated Hybrid Functionals. *J. Phys. Chem. B* **2019**, *123*, 8970−8975.

(21) Aksu, H.; Schubert, A.; Bhandari, S.; Yamada, A.; Geva, E.; Dunietz, B. D. On the Role of the Special Pair in Photosystems as a Charge Transfer Rectifier. *J. Phys. Chem. B* **2020**, *124*, 1987−1994.

(22) Begam, K.; Bhandari, S.; Maiti, B.; Dunietz, B. D. Screened Range-Separated Hybrid Functional with Polarizable Continuum Model Overcomes Challenges in Describing Triplet Excitations in the Condensed Phase Using TDDFT. *J. Chem. Theory Comput.* **2020**, *16*, 3287.

(23) Tinnin, J.; Bhandari, S.; Zhang, P.; Aksu, H.; Maiti, B.; Geva, E.; Dunietz, B. D.; Sun, X.; Cheung, M. S. Molecular-Level Exploration of the Structure-Function Relations Underlying Interfacial Charge Transfer in the Subphthalocyanine/C_{60} Organic Photovoltaic System. *Phys. Rev. Applied* **2020**, *13*, 054075.

(24) Aksu, H.; Maiti, B.; Ptaszek, M.; Dunietz, B. D. Photoinduced Charge Transfer in Zn and Au-Ligated Symmetric and Asymmetric Bacteriochlorin Dyads: A Computational Study. *J. Chem. Phys.* **2020**, *153*, 134111.

(25) Han, J.; Zhang, P.; Aksu, H.; Maiti, B.; Sun, X.; Geva, E.; Dunietz, B. D.; Cheung, M. On the Interplay Between Electronic Structure and Polarizable Force Fields When Calculating Solution-Phase Charge Transfer Rates. *J. Chem. Theory Comput.* **2020**, *16*, 6481−6490.

(26) Cammi, R.; Tomasi, J. Nonequilibrium Solvation Theory for the Polarizable Continuum Model: A New Formulation at the SCF Level with Application to the Case of the Frequency-Dependent Linear Electric Response Function. *Int. J. Quantum Chem.* **1995**, *56*, 465−474.

(27) Cossi, M.; Barone, V. Separation Between Fast and Slow Polarizations in Continuum Solvation Models. *J. Phys. Chem. A* **2000**, *104*, 10614−10622.
(28) Improta, R.; Barone, V.; Scalmani, G.; Frisch, M. J. A State-Specific Polarizable Continuum Model Time Dependent Density Functional Theory Method for Excited State Calculations in Solution. *J. Chem. Phys.* **2006**, *125*, 054103.
(29) Cammi, R. Coupled-Cluster Theories for the Polarizable Continuum Model. II. Analytical Gradients for Excited States of Molecular Solutes by the Equation of Motion Coupled-Cluster Method. *Int. J. Quantum Chem.* **2010**, *110*, 3040−3052.
(30) Zimmerman, G.; Chow, L.-Y.; Paik, U.-J. The Photochemical Isomerization of Azobenzene. *J. Am. Chem. Soc.* **1958**, *80*, 3528.
(31) Bandara, H. M. D.; Burdette, S. C. Photoisomerization in Different Classes of Azobenzene. *Chem. Soc. Rev.* **2012**, *41*, 1809.
(32) Wang, F.; Liu, X.; Willner, I. DNA Switches: from Principles to Applications. *Angew. Chem., Int. Ed.* **2015**, *54*, 1098.
(33) Beharry, A. A.; Sadovski, O.; Woolley, G. A. Azobenzene Photoswitching Without Ultraviolet Light. *J. Am. Chem. Soc.* **2011**, *133*, 19684.
(34) Velema, W. A.; Van Der Berg, J. P.; Hansen, M. J.; Szymanski, W.; Driessen, A. J.; Feringa, B. L. Optical Control of Antibacterial Activity. *Nat. Chem.* **2013**, *5*, 924.
(35) Matsunaga, D.; Asanuma, H.; Komiyama, M. Photoregulation of RNA Digestion by RNase H with Azobenzene-Tethered DNA. *J. Am. Chem. Soc.* **2004**, *126*, 11452.
(36) Siewertsen, R.; Neumann, H.; Buchheim-Stehn, B.; Herges, R.; Näther, C.; Renth, F.; Temps, F. Highly Efficient Reversible Z-E Photoisomerization of a Bridged Azobenzene with Visible Light through Resolved S1 (n-π*) Absorption Bands. *J. Am. Chem. Soc.* **2009**, *131*, 15594.
(37) Kshirsagar, A. R.; D'Avino, G.; Blase, X.; Li, J.; Poloni, R. Accurate Prediction of the S1 Excitation Energy in Solvated Azobenzene Derivatives via Embedded Orbital-Tuned Bethe-Salpeter Calculations. *J. Chem. Theory Comput.* **2020**, *16*, 2021−2027.
(38) Chai, J.-D.; Head-Gordon, M. Long-Range Corrected Hybrid Density Functionals With Damped Atom-Atom Dispersion Corrections. *Phys. Chem. Chem. Phys.* **2008**, *10*, 6615.
(39) Mewes, J.-M.; You, Z.-Q.; Wormit, M.; Kriesche, T.; Herbert, J. M.; Dreuw, A. Experimental Benchmark Data and Systematic Evaluation of Two a Posteriori, Polarizable-Continuum Corrections for Vertical Excitation Energies in Solution. *J. Phys. Chem. A* **2015**, *119*, 5446−5464.
(40) https://depts.washington.edu/eooptic/linkfiles.
(41) Rohrdanz, M. A.; Martins, K. M.; Herbert, J. M. A Long-Range-Corrected Density Functional That Performs Well for Both Ground-State Properties and Time-Dependent Density Functional Theory Excitation Energies, Including Charge-Transfer Excited States. *J. Chem. Phys.* **2009**, *130*, 054112−054119.
(42) Livshits, E.; Baer, R. A Well-Tempered Density Functional Theory of Electrons in Molecules. *Phys. Chem. Chem. Phys.* **2007**, *9*, 2932−41.
(43) Stein, T.; Kronik, L.; Baer, R. Reliable Prediction of Charge Transfer Excitations in Molecular Complexes Using Time-Dependent Density Functional Theory. *J. Am. Chem. Soc.* **2009**, *131*, 2818.
(44) Kronik, L.; Stein, T.; Refaely-Abramson, S.; Baer, R. Excitation Gaps of Finite-Sized Systems from Optimally Tuned Range-Separated Hybrid Functionals. *J. Chem. Theory Comput.* **2012**, *8*, 1515−1531.
(45) Phillips, H.; Geva, E.; Dunietz, B. D. Calculating Off-Site Excitations in Symmetric Donor-Acceptor Systems Via Time-Dependent Density Functional Theory With Range-Separated Density Functionals. *J. Chem. Theory Comput.* **2012**, *8*, 2661−2668.
(46) Phillips, H.; Zheng, Z.; Geva, E.; Dunietz, B. D. Orbital Gap Predictions for Rational Design of Organic Photovoltaic Materials. *Org. Electron.* **2014**, *15*, 1509−1520.
(47) Bhandari, S.; Zheng, Z.; Maiti, B.; Chuang, C.-H.; Porel, M.; You, Z.-Q.; Ramamurthy, V.; Burda, C.; Herbert, J. M.; Dunietz, B. D. What Is the Optoelectronic Effect of the Capsule on the Guest Molecule in Aqueous Host/Guest Complexes? A Combined Computational and Spectroscopic Perspective. *J. Phys. Chem. C* **2017**, *121*, 15481−15488.
(48) Hu, Z.; Zhou, B.; Sun, Z.; Sun, H. Prediction of Excited-State Properties of Oligoacene Crystals Using Polarizable Continuum Model-Tuned Range-Separated Hybrid Functional Approach. *J. Comp. Chem. J. Comp. Chem.* **2017**, *38*, 569.
(49) Yanai, T.; Tew, D. P.; Handy, N. C. A New Hybrid Exchange-Correlation Functional Using Coulomb-Attenuating Method (CAM-B3LYP). *Chem. Phys. Lett.* **2004**, *393*, 51−57.
(50) Genova, A.; Ceresoli, D.; Krishtal, A.; Andreussi, O.; DiStasio, R. A., Jr; Pavanello, M. eQE: An Open-Source Density Functional Embedding Theory Code for the Condensed Phase. *Int. J. Quantum Chem.* **2017**, *117*, e25401.
(51) Mi, W.; Shao, X.; Genova, A.; Ceresoli, D.; Pavanello, M. eQE 2.0: Subsystem DFT beyond GGA Functionals. *Comput. Phys. Commun.* **2021**, *269*, 108122.
(52) Perdew, J. P.; Burke, K.; Ernzerhof, M. Generalized Gradient Approximation Made Simple. *Phys. Rev. Lett.* **1996**, *77*, 3865.
(53) Laricchia, S.; Fabiano, E.; Constantin, L. A.; Della Sala, F. Generalized Gradient Approximations of the Noninteracting Kinetic Energy from the Semiclassical Atom Theory: Rationalization of the Accuracy of the Frozen Density Embedding Theory for Nonbonded Interactions. *J. Chem. Theory Comput.* **2011**, *7*, 2439−2451.
(54) Kaminski, J. W.; Gusarov, S.; Wesolowski, T. A.; Kovalenko, A. Modeling Solvatochromic Shifts Using the Orbital-Free Embedding Potential at Statistically Mechanically Averaged Solvent Density. *J. Phys. Chem. A* **2010**, *114*, 6082−6096.
(55) Laktionov, A.; Chemineau-Chalaye, E.; Wesolowski, T. A. Frozen-Density Embedding Theory with Average Solvent Charge Densities From Explicit Atomistic Simulations. *Phys. Chem. Chem. Phys.* **2016**, *18*, 21069.
(56) Scholz, L.; Tölle, J.; Neugebauer, J. Analysis of Environment Response Effects on Excitation Energies Within Subsystem-Based Time-Dependent Density-Functional Theory. *Int. J. Quantum Chem.* **2020**, *120*, e26213.
(57) Niemeyer, N.; Tölle, J.; Neugebauer, J. Approximate versus Exact Embedding for Chiroptical Properties: Reconsidering Failures in Potential and Response. *J. Chem. Theory Comput.* **2020**, *16*, 3104−3120.
(58) You, Z.-Q.; Mewes, J.-M.; Dreuw, A.; Herbert, J. M. Comparison of the Marcus and Pekar Partitions in the Context of Non-Equilibrium, Polarizable-Continuum Solvation Models. *J. Chem. Phys.* **2015**, *143*, 204104.
(59) Mewes, J.-M.; Herbert, J. M.; Dreuw, A. On the Accuracy of the State-Specific Polarizable Continuum Model for the Description of Correlated Ground and Excited States in Solution. *Phys. Chem. Chem. Phys.* **2017**, *19*, 1644−1654.
(60) Epifanovsky, E.; Gilbert, A. T. B.; Feng, X.; Lee, J.; Mao, Y.; Mardirossian, N.; Pokhilko, P.; White, A. F.; Coons, M. P.; Dempwolff, A. L.; et al. Software for the frontiers of quantum chemistry: An overview of developments in the Q-Chem 5 package. *J. Chem. Phys.* **2021**, *155*, 084801.
(61) Cammi, R.; Mennucci, B. Linear Response Theory for the Polarizable Continuum Model. *J. Chem. Phys.* **1999**, *110*, 9877−9886.
(62) Bhandari, S.; Sarkar, S.; Schubert, A.; Yamada, A.; Payne, J.; Ptaszek, M.; Geva, E.; Dunietz, B. D. Intersystem Crossing in Tetrapyrrolic Macrocycles. A First Principles Analysis. *J. Phys. Chem. C* **2021**, *125*, 13493.
(63) Knie, C.; Utecht, M.; Zhao, F.; Kulla, H.; Kovalenko, S.; Brouwer, A. M.; Saalfrank, P.; Hecht, S.; Bléger, D. ortho-Fluoroazobenzenes: Visible Light Switches with Very Long-Lived Z Isomers. *Chem. Eur. J.* **2014**, *20*, 16492−16501.
(64) Ohio Supercomputer Center. 1987. http://osc.edu/ark:/19495/f5s1ph73 (accessed on 01-01-2014).

https://doi.org/10.1021/acs.jpclett.2c00982
J. Phys. Chem. Lett. 2022, 13, 4849−4855